Journal of Applied Polymer Science

Electrospun poly(vinyl alcohol) composite nanofibers with halloysite nanotubes for the sustained release of sodium D-pantothenate

Il Woo Lee,[1] Jinglei Li,[1] Xiguang Chen,[2] Hyun Jin Park[1]

[1]Department of Biotechnology, College of Life Sciences and Biotechnology, Korea University, 5-Ka, Anam-Dong, Sungbuk-Ku, Seoul 136-701, Republic of Korea

[2]College of Marine Life Science, Ocean University of China, Qingdao 266003, Shandong, People's Republic of China

Correspondence to: H. J. Park (E-mail: hjpark@korea.ac.kr)

ABSTRACT: Poly(vinyl alcohol) (PVA) nanofibers containing halloysite nanotubes (HNTs) loaded with sodium D-pantothenate (SDP) were successfully fabricated via simple blend-electrospinning. SDP was efficiently loaded into the innate HNT lumen with an SDP/HNT mass ratio of 1.5:1 via vacuum treatment. The SDP-loaded HNT-inclusion complex was evaluated with drug-loading efficiency testing, Fourier transform infrared (FTIR) spectroscopy, and X-ray diffraction. The morphologies of the nanofibers were observed by scanning electron microscopy, which revealed uniform and smooth surfaces of the nanofibers. The addition of HNTs to the composite nanofibers increased the viscosity of the polymer solution, and this suggested shorter fiber diameters. FTIR spectroscopy verified the good compatibility of the SDP and HNTs with PVA. Moreover, the swelling properties were found to quantitatively correlate with weight loss. *In vitro* drug-release testing revealed that the HNTs and crosslinking reaction most dramatically affected the sustained release of SDP from the PVA and SDP-loaded HNT complex. In the drug-release kinetics model, SDP release depended on the diffusion caused by the deformation of the polymer-based structures in the medium; it followed Fickian diffusion with acceptable coefficient of determination (r^2) values between 0.88 and 0.94. Most importantly, the HNTs as natural biocontainers effectively modulated the release profile by loading the active compound in harmony with the electrospun nanofibers. © 2015 Wiley Periodicals, Inc. J. Appl. Polym. Sci. **2016**, *133*, 42900.

KEYWORDS: drug-delivery systems; electrospinning; hydrophilic polymers; nanostructured polymers

Received 7 May 2015; accepted 29 August 2015

DOI: 10.1002/app.42900

INTRODUCTION

Electrospinning is a versatile method that transforms a polymer solution emitted from a jet into a fibrous mat with fibers ranging from the microscale to the nanoscale by hierarchically elaborated formation.[1] Uniform and smooth fibers are fabricated according to the relationship between the surface tension of the polymer melt or solution and the electrostatic forces generated by a direct power voltage, which are the two major forces present in electrospinning.[2] The system's particular three-dimensional structure endows the electrospun nanofibrous mats with an extremely high specific surface area, a readily tunable porous matrix, and a capacity for modulation to meet the desired requirements for various purposes.[3,4]

Controlled drug-delivery systems have steadily gained much interest for treating many diseases.[5] In the field of drug delivery, the transdermal drug-delivery system (TDDS) fabricated by either natural or synthetic polymers is a pinpoint technology intended to achieve necessary effects with specific drugs, where the drug's effects can be enhanced by polymers.[6] TDDS is also beneficial for conventional modes of drug administration, especially in improving patient compliance through prevention of direct treatment and the use of a minimal dosage of the target drug.[7] Conformations containing specific substances can be classified into two main categories. One method focuses on the attachment of the active substance to the surfaces of fibers, such as the immobilization of functionalized yeast[8] and cellulase[9] and the attachment of silver nanoparticles.[10] The other method involves the loading of the active compound into biocontainers, such as polysaccharide-derived cyclodextrin loaded with geraniol,[11] silica containing ibuprofen as an inorganic nanoparticle,[12] and halloysite nanotubes (HNTs), obtained from natural inorganic compounds, loaded with tetracycline hydrochloride.[13]

Natural biocontainers have gained widespread interest in research on biofunctional foods, pharmaceutics, catalysts, and filtration, as their safety is better than that of synthetic materials. From the research conducted in the field of drug delivery, HNTs are aluminosilicate nanotubes with a cylindrical shape

obtained from naturally abundant clay minerals.[14] They consist of two parts: the external shell and the internal lumen, with diameters of about 50 and 15 nm, respectively. The length of the HNTs ranged approximately from 300 to 800 nm.[15] Because of the structure's lumen, the HNTs were feasible for entrapping targeted drugs,[16] enzymes such as α-amylase and urease,[17] protective agents,[18] and anticorrosion coatings.[19] Therefore, in this study, HNTs were chosen as loading agents.

Poly(vinyl alcohol) (PVA) is a water-soluble synthetic polymer that is nontoxic,[20] biocompatible,[21] and biodegradable.[22] With its strong resistance to chemical and thermal treatments, PVA resin and chemically modified hydrogels have been used for many applications.[23] PVA has many active hydroxyl groups adhered to its carbon chain in a pendant shape, so it requires chemical or physical crosslinking before use in many applications.[24] TDDSs composed of PVA with various average molecular weights have been developed for chemicals or drugs, such as curcumin;[25] sodium salicylate, diclofenac sodium, naproxen, and indomethacin (the latter two of which are insoluble in water);[26] metoprolol;[27] lidocaine; and prilocaine.[28] Another study reported the use of PVA nanofibers for adjusting the fast-dissolving oral delivery of caffeine and riboflavin.[29]

Sodium D-pantothenate (SDP; CAS No. 867-81-2) is a sodium salt of pantothenic acid, which is the precursor of vitamin B5 and the inactive form of coenzyme A.[30] Dexpanthenol, an alcohol analog of pantothenic acid, is used for commercial purposes, such as hair care treatments, ointments (Bepanthen, Bayer, United Kingdom), and artificial tears.[31] Because of its unique hygroscopic properties, SDP acts as a moisturizer, enhancing wound-healing rates.[32] SDP is readily soluble in deionized (DI) water; this makes it easy to handle and also guarantees that SDP can easily reach the HNT lumen.

We conclude that the presence of HNTs in PVA nanofibers may induce sustained SDP release; this is not the case with HNT-free electrospun PVA nanofibers. Crosslinking reactions may affect the morphology and surface of the PVA fibers in harmony with the HNTs. The aim of this study was to prepare a complex of PVA, SDP, and HNTs to understand their performance in developed TDDS. Our systematic study included the physical and chemical characterization of the properties of the complex; these properties included the morphology and average diameter, X-ray diffraction (XRD) patterns, IR spectra, drug-loading efficiency (DLE), porosity, swelling ratio, weight loss, and *in vitro* drug release. The amounts of SDP and HNTs were also measured to determine the most efficient ratio for the loading of the HNTs with SDP. The pivotal focus in our study was the investigation of the suitability of the HNTs as biocontainers for active materials.

EXPERIMENTAL

Materials

PVA, with a degree of polymerization of 1500, was purchased from Showa Chemical Co., Ltd. (Tokyo, Japan). SDP, supplied by Tokyo Chemical Industry Co., Ltd. (Tokyo, Japan), had a molecular weight of 241.22 g/mol (≥97.0%). The HNTs, originating from halloysite nanoclay, with a molecular weight of 294.13 g/mol, a specific gravity of 2.53, and a pore volume of 1.26–1.34 mL/g, were purchased from Sigma-Aldrich. A glutaraldehyde (GA) 25% v/v solution, which was used as a crosslinking agent with a molecular weight of 100.12 g/mol and a specific gravity of 1.065, was purchased from Junsei Chemical Co., Ltd. HCl in a typical 35–37% aqueous solution was supplied by Duksan Pure Chemical Co., Ltd. DI water was used as received as Aquamax-Ultra (Younglin Instrument Co., Ltd.) in all of the experiments. All of the reagents were commercial-grade materials and were used without further purification.

Nanofiber Composite Fabrication

Preparation of the Polymer Solutions. In the experiments, all of the samples, including SDP, either partially loaded into the HNTs [sodium D-pantothenate loaded halloysite nanotubes (SDP@HNTs)] or directly embedded into the PVA nanofibers, were compared with both SDP solely incorporated into PVA mats and pure PVA mats. First, the SDP@HNT composite was fabricated with various parameters, including the weight ratio of the SDP to HNTs and the SDP@HNT solution concentration, to determine the optimal SDP/HNTs ratio for DLE. Second, the fabricated SDP@HNT complex was added to the PVA solution, which was prepared by the immersion of 4 g of PVA into DI water at 10% w/v. For the non-HNT composites, SDP was added to 40 mL of a 10% w/v PVA solution; we adjusted the SDP concentration to the a PVA/SDP ratio of 20:1 w/w. The third step included the fabrication of a pristine PVA solution through the mixture of 4 g of PVA into 40 mL of DI water with vigorous magnetic stirring at 75°C for 3 h. The concentration of the prepared polymer solution was adjusted to 10% w/v. All of the samples were prepared before electrospinning.

Solution Viscosity Measurement. Before the polymer solutions were rendered into fibrous mats by electrospinning, the viscosity of the polymer blends was measured with a Brookfield digital viscometer (LVDV-IICP, Brookfield Engineering Laboratories, Inc., Middleborough, MA) at 25°C and 30 rpm. Each solution was sampled and measured three times; the average values from these tests are reported.

DLE. Before electrospinning, we evaluated DLE to identify the optimal loading conditions. The test, which was denoted as the double-loading process, was performed according to a previous publication with modifications.[13] In brief, SDP was dissolved in DI water with various SDP/HNT weight ratios of 1:2, 1:1, 3:2, and 2:1, with a fixed the amount of the HNTs at 200 mg/mL. The fully dried and sieved HNT powder was dispersed into the homogeneous SDP solution. This was followed by ultrasound sonication (VCX 750, Sonic & Materials, Inc., Newton, CT) for 30 min to further enhance the dispersion of the HNTs. To replace the inner volumes of air within the HNTs with SDP, the pressure was adjusted to 0.021 MPa by a vacuum pump for 30 min. After repeated stirring and at a reduced pressure, the composite solutions were centrifuged at 7000 rpm for 10 min in a Beckman centrifuge. After the supernatant was separated from the centrifuge tube, the precipitate was withdrawn and stored in a dry oven at 70°C for 1 day. The fully dried precipitate was added to the remaining supernatant to reduce costs. The drug-loaded SDP@HNT solutions were obtained through a repetition of the previous steps. DLE was calculated by high-performance

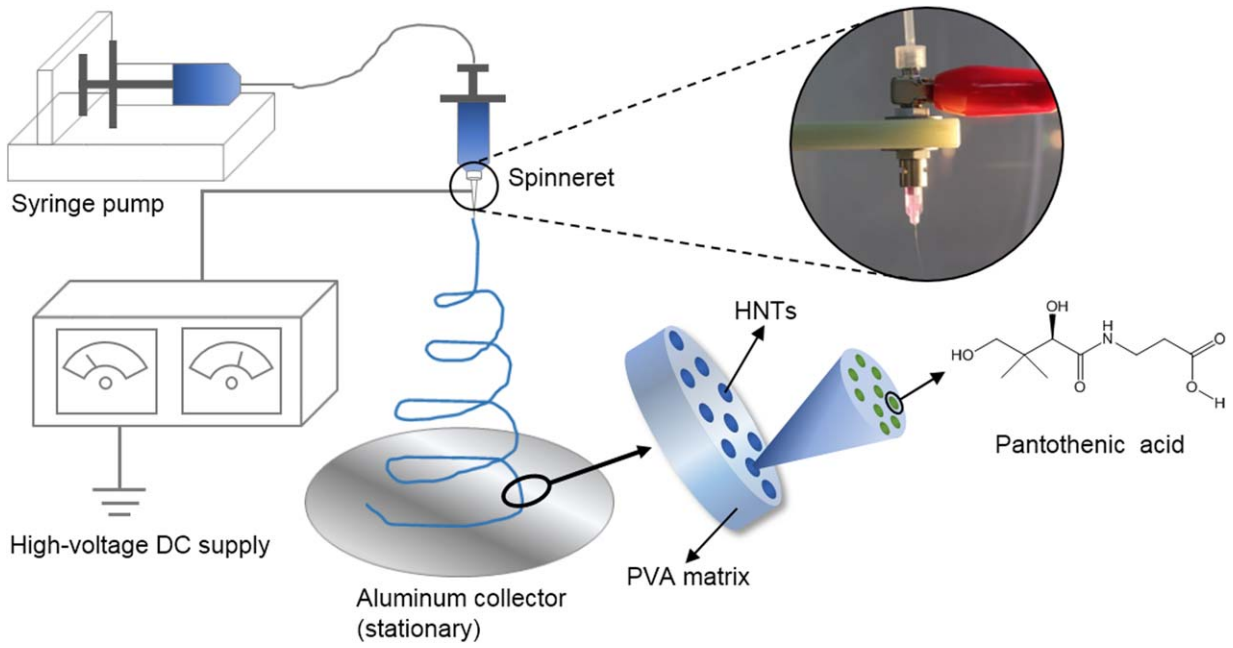

Figure 1. Schematic of the electrospinning apparatus, which was composed of a syringe pump, a spinneret, an aluminum collector, and an HV direct-current (DC) supply; detailed digital photograph of the single-jet spinneret; and structure of the PVA&SDP@HNT complex. [Color figure can be viewed in the online issue, which is available at wileyonlinelibrary.com.]

liquid chromatography (details given in the *In Vitro* Release from the Electrospun Fibers section) to determine the optimal SDP/HNTs ratio. DLE was determined with the following equation:

$$\text{DLE}\ (\%) = C_L/C_T \times 100\ (\%) \quad (1)$$

where C_L is the loaded amount of SDP and C_T is the total amount of dissolved SDP into DI water.

Electrospinning. For electrospinning, 5 mL of each of the previously prepared polymer solutions was carefully transferred to a 12-mL syringe (NORM-JECT, Henke Sass Wolf, Germany). The electrospinning apparatus consisted of a high-voltage (HV) generator, a syringe pump (KDS200), a manual *X*–*Y* table, and collector (ESP200, NanoNC, Korea). The syringe was connected with a polyethylene tube (*i.d.* = 2 mm) to a nozzle adapter, which connected the HV generator and a 30G needle (*i.d.* = 0.15 mm). The feed rate of the syringe pump was set at 0.125 mL/h, and the working distance from the spinneret to the aluminum plate collector was 13 cm under an applied voltage of 11.5 ± 0.5 kV. The ambient room temperature was regulated at 25°C with a relative humidity of 40%. The resulting fibers were collected in a circular shape on an aluminum plate collector. Figure 1 provides a more precise scheme of the electrospinning apparatus. After detachment from the aluminum collector, all of the samples were stored in a dry oven for 1 day to remove the residual solvent. Table I displays the electrospinning parameters used to prepare the nanofibers.

Crosslinking of the Electrospun Nanofibers. For the broader application of the PVA-based nanofibers, the crosslinking treatment of the electrospun PVA, poly(vinyl alcohol) and sodium D-pantothenate (PVA&SDP), and poly(vinyl alcohol) and sodium D-pantothenate loaded halloysite nanotube (PVA&SDP@HNT) nanofibers was conducted in a desiccator with a laboratory scale. Each electrospun fiber was crosslinked by storage in a desiccator with a mixture solution of 25% v/v GA and 35–37% v/v HCl for 1 day. HCl was used to create acidic conditions as a catalyst.[1] All of the crosslinked samples

Table I. Polymer Solution Parameters, Average Fiber Diameter Values, and Morphology of the Electrospun Nanofibers

Solution	Solvent	% PVA (w/v)[a]	% SDP (w/w)[b]	% HNTs (w/w)[b]	Spinning voltage (kV)	Viscosity (Pa s)	Average fiber diameter (nm)[c]	Fiber morphology
PVA	DI water	10	—	—	10.5 ± 0.5	333.08 ± 10.05	371 ± 81	Bead-free fibrous form
PVA/SDP	DI water	10	5	—	10.5 ± 1.0	352.67 ± 21.36	323 ± 67	Bead-free fibrous form
PVA/SDP@HNTs	DI water	10	5	3.33	10.5 ± 1.0	531.80 ± 35.99	234 ± 62	Bead-free fibrous form

The flow rate was 0.125 mL/h, and the working distance was 10 cm.
[a] With respect to the solvent (DI water).
[b] With respect to the polymer (PVA).
[c] Reported as the average plus or minus the standard deviation. For each case, 50 fibers were analyzed.

were washed in deionised water (DW) to remove residual GA and then dried in a dry oven for further use.

Characterization of the Electrospun Nanofibers

Morphological Characterization. The morphology of the electrospun nanofibers was evaluated by field emission scanning electron microscopy (S-4300, Hitachi, Tokyo, Japan) at an accelerating voltage of 15 kV. Before scanning electron microscopy (SEM) observation, all of the samples, with a mat size of 0.2 × 0.2 mm^2 were attached to metallic stubs with a double-adhesive-coated carbon tape (Ultra Smooth Carbon Tapes, Electron Microscopy Sciences, Hatfield, PA) and coated with platinum by ion sputtering for 90 s under a current of 15 mA and vacuum pressure (E-1030, Hitachi, Japan). At least 50 randomly selected positions on the SEM images of the nanofibrous mats were examined with image software (ImageJ, National Institutes of Health, Bethesda, MD) with original magnifications of 7000 (7KX); 20,000× (20KX) to determine the average diameter of the strand of nanofibers and the size distributions of the electrospun nanofibers.

Fourier Transform Infrared (FTIR) Spectroscopy. To examine the chemical structural characteristics of the fabricated SDP@HNT composite, the FTIR spectra of both nanofibrous mats and the raw materials were recorded. Briefly, 2 mg of the as-prepared nanofibers was mixed with 200 mg of dried potassium bromide (0.01 mg/mg), ground, and compressed into a tablet via the application of 10 tons in a hydraulic press; the tablet was used for FTIR spectral examination on a Varian 640 FTIR spectrometer (Agilent Technologies, Santa Clara, CA). The thickness of the potassium bromide pellet was 0.5 mm. Each spectrum was obtained by the averaging of 30 scans taken at a resolution of 2 cm^{-1} in the range 650–4000 cm^{-1}.

XRD. The electrospun samples were measured with an X-ray diffractometer (X'Pert PW3040/00, Philips, Almelo, The Netherlands) with Cu Kα radiation with a K-A2/K-A1 ratio of 0.5 at 30 mA and 40 kV. The scanning ranges for the powder-type samples and fiber mats were 5–50 and 5–80°, respectively, with a step size of 0.04° at a scan rate of 1.2°/min. Approximately 1 cm^2 of the electrospun mat and powder, attached to a standard sample holder, was used for diffraction measurements.

Porosity of the Nanofibers. The thickness of the electrospun mat was measured with a micrometer (model 674, range = 10.00 mm, Hans Baer, Zurich, Switzerland) and was found to range from 300 to 360 μm. Before the measurements, all of samples (stored in a dry oven for 1 day) were cut to dimensions of 10 × 10 mm^2 for simplified calculations. The apparent density and porosity of the nanofibers were calculated according to the following previously described equations from the literature:[33,34]

$$\text{NFM apparent density}\left(\frac{\text{g}}{\text{cm}^3}\right) = \frac{\text{NFM mass}(\text{mg} \times 10)}{\text{NFM thickness}(\mu\text{m}) \times \text{NFM area}(\text{cm}^2)} \quad (2)$$

$$\text{NFM porosity}(\%) = \left[1 - \frac{\text{NFM apparent density}\left(\frac{\text{g}}{\text{cm}^3}\right)}{\text{Bulk density of the polymer solution}\left(\frac{\text{g}}{\text{cm}^3}\right)}\right] \times 100$$

where NFM is the nanofiber mat. The bulk densities of the PVA, PVA&SDP, and PVA&SDP@HNT solutions were 1.048, 1.039, and 1.041 g/cm^3, respectively, at 25°C.

Swelling Ratio and Weight Loss. The swelling ratio of the crosslinked unloaded PVA and loaded PVA&SDP and PVA&SDP@HNT mats were measured with the following equation:[35]

$$\text{Swelling ratio } (\%) = (M_s - M_d)/M_d \times 100 \quad (3)$$

where M_s is the weight of the swollen nanofiber mat, which was prepared by the dabbing of the surface of the nanofiber scaffolds with filter paper before they were weighed, and M_d is the dried weight after the immersion of the sample in a phosphate-buffered saline (PBS) medium at pH 7.4 and 37°C in an agitated water bath for 12 h. It was measured after the swollen nanofibrous mats were dried in a dry oven at 75°C until a constant weight was maintained. The weight loss of all of the samples was simultaneously measured by the following equation:

$$\text{Weight loss } (\%) = (M_i - M_d)/M_i \times 100 \quad (4)$$

where M_i is the initial dry mass of the sample. The method is the same as that in the aforementioned [eq. (3)].

In Vitro Release from the Electrospun Fibers

The *in vitro* release of the model drug (SDP) from the electrospun scaffolds was evaluated with SDP@HNT and SDP-embedded nanofibers with and without crosslinking in proper aqueous solutions with three replicates for each scaffold. All of the samples, weighing 2.5 mg, were completely immersed in PBS for 8 days. The samples were kept in a water bath with constant stirring (75 rpm) at a temperature of 37°C. At predetermined time intervals from 5 min to 8 days, a 1-mL aliquot was withdrawn and replaced with the same amount of DI water to maintain a constant 10-mL volume. The SDP concentrations in the withdrawn aliquots were determined by high-performance liquid chromatography with a Hewlett Packard 1100 system (Agilent 1100, Agilent Technologies) equipped with a degasser (G1379A), autosampler (G1313A), quaternary pump (G1311A), and an UV–visible diode array (G1315A).

To analyze the *in vitro* release kinetics, the release profile of the drug from the electrospun nanofibers was calculated by the Korsmeyer–Peppas kinetic model.[36] The data obtained from the release profiles were plotted versus the time, which was set as programmed intervals. The Korsmeyer–Peppas equation is as follows:

$$M_t/M_\infty = Kt^n \quad (5)$$

where K, n, t, and M_t/M_∞ are the characteristic constant incorporating the structural and geometric characteristics of the drug, the release exponent showing the drug-release mechanism, the time, and the fraction of drug release at specific time t, respectively.

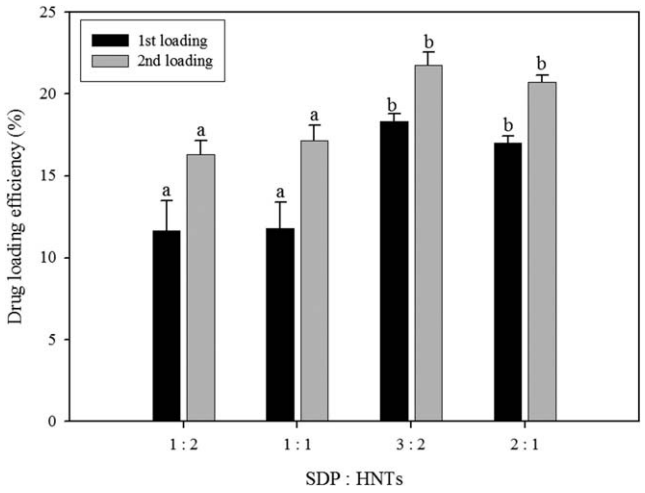

Figure 2. DLE for the optimal mass ratio of SDP to HNTs (fixed at 5 mg/mL). Different letters (a and b) within a column indicate significant differences ($p < 0.05$) according to a Duncan's multiple-range test.

Statistical Analysis

All of the experiments were carried out in triplicate, and all of the values recorded are presented as means and standard deviations. A one-way analysis of variance and a Duncan's multiple-range test were used for the statistical analysis of the data. The results were statistically obtained through the available SPSS software package (SPSS 20.0, IBM, Chicago, IL). In all analyses, the significance was defined at $p < 0.05$.

RESULTS AND DISCUSSION

It was necessary to determine DLE for the following step (fabricating nanofibers) in our study. With the DLE test results, we achieved a 3:2 (300:200) SDP@HNT complex with the optimal mass ratio. With a fixed amount of HNTs, higher concentrations correlated to more SDP attaching to the surfaces of the HNTs. However, in case of too high a concentration of SDP, the amount of residual SDP in the solution increased, and this corresponded to a lower loading efficiency.[13] DLE depended on the state of the inherent lumen and dispersion of the HNTs, whereas *in vacuo,* water molecules and air were withdrawn from the lumen of sufficiently dispersed HNTs, and then, SDP took their place. DLE was relatively low at 10–20% (Figure 2), and this was attributed to the precipitation and aggregation of the HNTs. In the continuous aggregation and dispersion of the HNTs, when SDP occupied the lumen, more air entered the lumen and thus caused a low SDP loading.[13]

Fabrication of the Polymer and Drug-Inclusion Complex

SEM analysis revealed a nanoscale mean diameter and a uniform fibrous morphology in all of the samples. A strand of each fabricated nanofiber generally showed a smooth surface morphology, as depicted in the insets of Figure 3. In panel B, some thinner fibers between normal fibers are shown; these formed generally formed subfibers, which were introduced by Oh *et al.*,[37] who focused on meta-aramid polymers. As shown in panel C, some beads attached to the surface of the nanofibers displayed a hump-shaped formation. A similar pattern was also

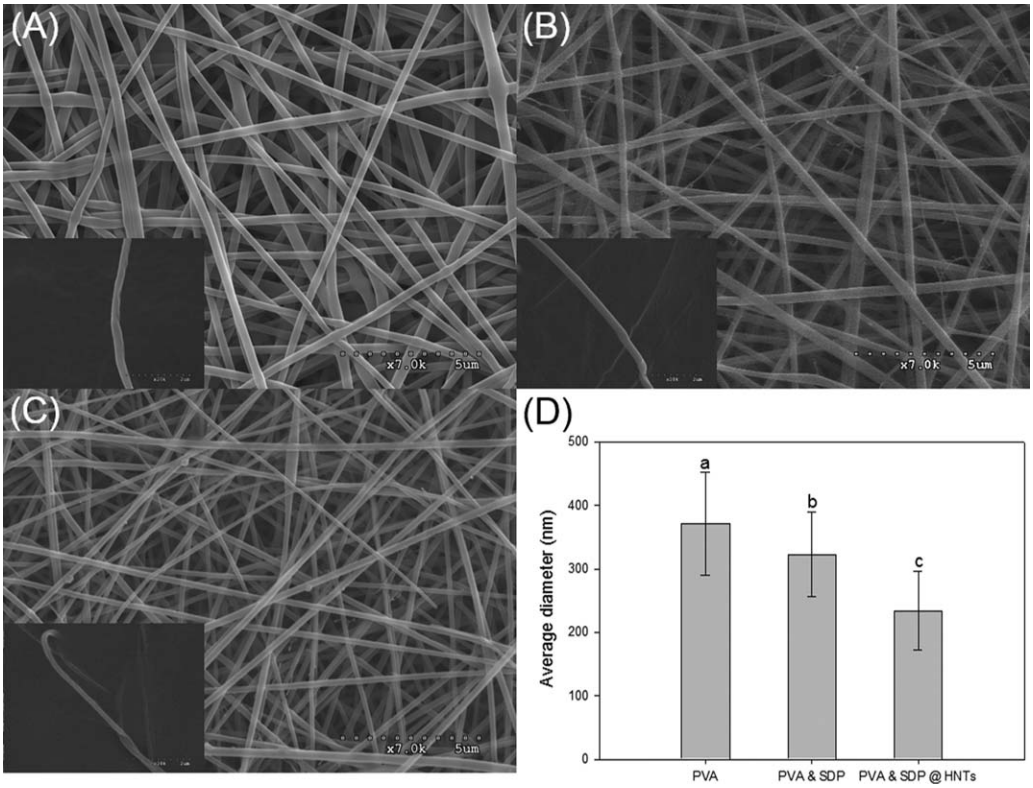

Figure 3. SEM images of (a) PVA, (b) PVA&SDP, and (c) PVA&SDP@HNT nanofibers. The insets show high-magnification SEM micrographs (20,000×) of a strand of each nanofiber. (D) Corresponding average diameter of the as-electrospun nanofibers.

shown by Fu *et al.*,[38] where some aggregated core materials were observed in the electrospun scaffold. The average fiber diameter of the three tested fiber types showed a statistically significant difference ($p < 0.05$). To investigate the relationship between the viscosity of the polymer solutions and the fiber diameter of the electrospun nanofibers, we conducted viscosity measurements. The viscosities of the as-prepared polymer solutions of PVA, PVA&SDP, and PVA&SDP@HNTs were 333.09 ± 10.05, 352.67 ± 21.35, and 531.8 ± 35.99 cP, respectively, at 25°C at 30 rpm. Higher viscosity polymer solutions were correlated with smaller fiber diameters. When electrospun, the HNT-containing polymer solution produced an irregular fiber structure with some beads because of its higher viscosity. The lower fiber diameter indicated that the HNTs hindered uniform fiber formation from the PVA&SDP@HNT complex. The excessive increase in the chain entanglement caused by the HNTs posed difficulties in the production of a uniform nanofiber. This tendency was evident between the mean diameter of the fibers and the measured viscosity in a series of studies on the fabrication of nanofibers.[4,39]

FTIR Analysis of the Nanofibers

Figure 4 shows the FTIR spectra of the SDP, HNTs, and SDP@HNTs as incorporated composites [Figure 4(A)] and PVA, PVA&SDP that did not contain HNTs, and PVA&SDP@HNTs [Figure 4(B)]. The FTIR spectrum of the HNTs displayed two conspicuous peaks at 3698 and 3623 cm^{-1}; these were attributed to inner Al_2OH (or Al—OH) group stretching and the internal surface of the HNTs. A peak at 913 cm^{-1} was assigned to the bending band of the Al—OH groups.[16] A weak peak at 2972 cm^{-1} was assigned to CH_3 stretching.[40] The bands at 1085 and 1026 cm^{-1} are due to the presence of Si—O bands causing plane vibration.[41] Two weak peaks at 789 and 749 cm^{-1} were attributed to both out-of-plane O—H bending and external O—H groups.[40]

The FTIR spectrum of SDP alone displayed numerous peaks. A broad peak at 3550–3200 cm^{-1} and two sharp peaks at 3442 and 3396 cm^{-1} were attributed to steric hindrance, which prevented hydrogen bonding, by functional groups such as N—H.[40] A peak at 3271 cm^{-1} corresponded to secondary amide C=O stretching. The peaks located from 2962 to 2855 cm^{-1} correlated to C—H bond stretching. Peaks identifying COO^- asymmetrical bending and C—N—H bending at 1550 and 1250 cm^{-1}, respectively, were observed. As evident from the spectrum of SDP, several peaks were suppressed or disappeared after SDP was loaded into the HNTs.

In the case of SDP@HNTs, denoted as modified HNTs, inherent peaks at 3698 and 3623 cm^{-1} indicating Al—OH stretching were maintained from the spectrum of the raw HNTs. However, a new peak indicating symmetric CH_2 stretching of the modified HNTs at 2925 cm^{-1} appeared in the FTIR spectrum. This confirmed the presence of SDP on the surface of the HNTs. This observation corresponded to other research.[42,43]

To determine the structural changes in the nanofibrous mats and in the types of powder, the FTIR spectra of the three types of mat samples were measured. In contrast to the results of PVA, a new characteristic peak at 1574 cm^{-1}, indicating secondary acyclic amides, appeared after the addition of SDP into PVA; this indicated the homogeneous incorporation of SDP and PVA.[40] This peak resulted from interactions between the N—H

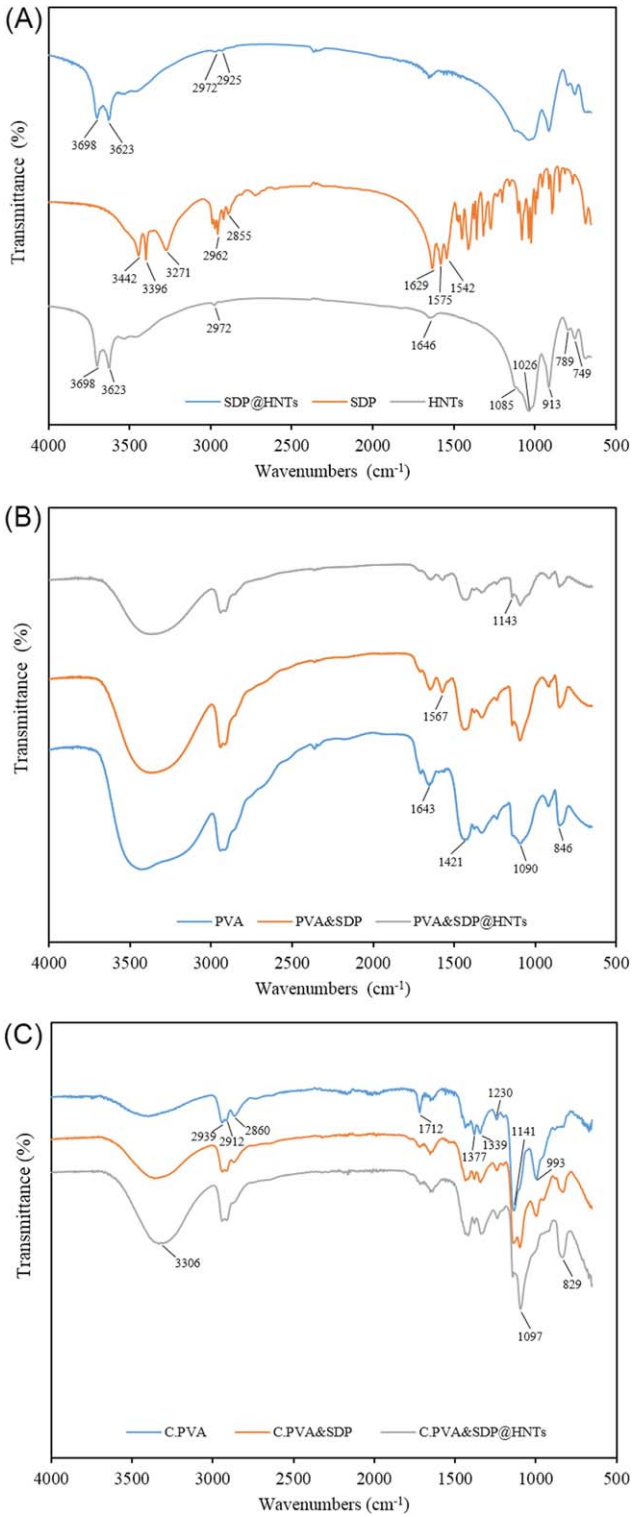

Figure 4. FTIR spectra of the (a) SDP@HNTs as an inclusion complex, SDP, and HNTs, (b) PVA, PVA&SDP, and PVA&SDP@HNT nanofibers, and (c) crosslinked nanofibers. [Color figure can be viewed in the online issue, which is available at wileyonlinelibrary.com.]

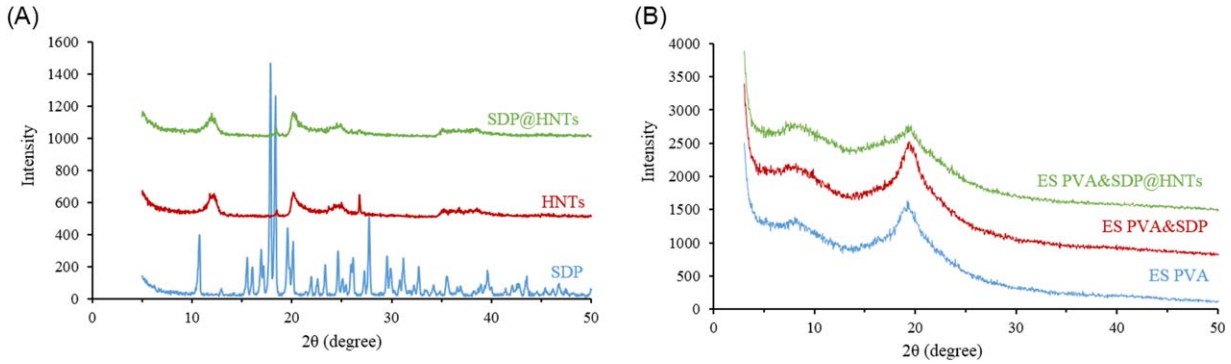

Figure 5. XRD diffraction patterns of the (a) SDP, HNTs and SDP@HNT complex and (b) electrospun (ES) PVA, PVA&SDP, and PVA&SDP@HNT nanofibers. [Color figure can be viewed in the online issue, which is available at wileyonlinelibrary.com.]

bending and C—N stretching of the C—N—H groups. A second weak peak at 1143 cm^{-1} was attributed to C—N stretching vibrations in the aliphatic amine.[44] This peak showed a suppressed formation relative to those of the PVA&SDP nanofiber. It seemed that the SDP loaded into the HNTs was affected by the inherent structure of the HNTs; this hindered the production of an FTIR spectrum of PVA&SDP@HNTs and induced somewhat lower peak intensities. We obtained similar results when observing the sample in both powder and mat forms. These results indicate that SDP was well loaded into the HNTs in the PVA structures; this was in line with the formation of an SDP@HNT inclusion complex.

As for the crosslinked samples [Figure 4(C)], a deeply broad peak at 3306 cm^{-1} for crosslinked poly(vinyl alcohol) and sodium D-pantothenate loaded halloysite nanotubes (C PVA&SDP@HNTs) was attributed to intramolecular and intermolecular hydrogen binding.[40] This result might have been a chemically connected interaction between the outer surface of the HNTs and the —OH groups of PVA in advance.

The remarkable peak at 1712 cm^{-1} of crosslinked poly(vinyl alcohol) (C PVA) was due to C=O stretching.[8] This peak was evidence that proved the crosslinking reaction, especially at the unacted end of GA, between the PVA nanofibers and GA. However, in the case of the crosslinked poly(vinyl alcohol), sodium D-pantothenate (C PVA&SDP), and C PVA&SDP@HNTs, the peak indicating C=O stretching tended to decrease. This decreased because the —OH groups of PVA already formed covalent linkages with the SDP and HNTs, and then, the active sites for the unreacted end of GA was decreased.

In the FTIR spectrum of the C PVA&SDP@HNTs, the evidence of chemical interactions between the composite fiber and GA were proven by enhanced two peaks, which indicated Si—O—C stretching at 1097 cm^{-1} [41] and Al—O—C stretching at 829 cm^{-1};[45] this was in line with the crosslinking reaction with GA, which was also conducted with the composite nanofibers.

XRD Patterns

Figure 5(A) displays XRD patterns of the SDP@HNT complex, raw SDP, and HNTs as powder compounds. The XRD patterns for SDP demonstrated the crystallinity of the material; its representative peaks appeared at 10.74, 17.86, and 18.38° among many other peaks. With HNT powder, three distinct peaks at 12.26, 20.1, and 26.82° were observed with corresponding basal *d*-spacings of 7.33, 4.41, and 3.33 Å, respectively; these were similar to those described by Churchman and Theng.[46] In the powdered HNTs loaded with SDP, denoted as SDP@HNTs, the HNT peak at 26.74° completely disappeared, and most peaks of SDP were reduced or partially removed. The result was in agreement the results of Guo *et al.*,[47] where they reported that curcumin, a hydrophobic drug, changed in the amorphous form and was not a crystalline material. These changes suggest that the basal *d*-spacing of the HNT layers has a partially ordered layer structure in the SDP@HNT complex[48] and that some SDP is loaded into the cylindrical layers of the HNTs, by the previously described methods. The disappearance of the 26.74° peak was attributed to the replacement of the inherent monolayer of water molecules (ca. 3Å) by SDP via the applied vacuum treatment during the loading process.[14]

As shown in Figure 5(B), all of the samples containing PVA showed generally smooth lines in the XRD patterns and an appreciable peak at 19.54°, which indicated the inherently semicrystalline structure.[49] The three kinds of mats showed similar patterns with slightly small but noticeable differences in the peak intensities. In the PVA&SDP nanofibrous mats, these results were attributed to intermolecular hydrogen bonding, which originated from PVA and SDP being well dissolved in DI water; this caused increased mutual adherence and thus high-intensity XRD peaks. By contrast, the XRD patterns for the PVA&SDP@HNT nanofibers were lowest in intensity and broadest in the three types of samples. This implied that the HNTs in the composite structure enhanced intercalation, compared to the nanofibers that were not treated with the HNTs.[50]

Porosity of the Fabricated Nanofibers

We attempted to measure the porosity of the electrospun nanofibers to clarify our results. In the case of PVA versus PVA&SDP, the porosity did not differ significantly, whereas the porosity of the electrospun mat containing HNTs in the polymer matrix was significantly reduced. The PVA&SDP@HNT complex mat was opaque in appearance, unlike the other mats, and this confirmed the uniform dispersion of SDP@HNTs in the porous structure of the polymer matrix (Figure 6).

The porosity of all of the crosslinked nanofibers was significantly enhanced. Generally, the porosity was dependent on the

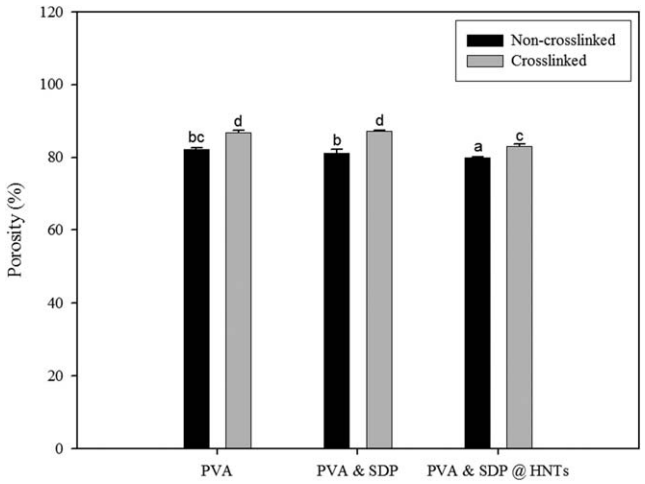

Figure 6. Porosity of the noncrosslinked and crosslinked nanofibrous mats. Different letters (a–d) within a column indicate significant differences ($p < 0.05$).

apparent density. Under the same surface area of nanofibers at 1 cm^2, the thickness affected the apparent density. In other words, the high-thickness nanofibrous mat had a relatively low apparent density. According to eqs. (2) and (3), the apparent density of the noncrosslinked nanofibers was higher than those of the crosslinked ones. Similar results were reported by Affandi *et al.*,[51] who reported that the thickness of the PVA nanofibers increased after the crosslinking reaction. This phenomena was elucidated by the presence of GA in the PVA-based nanofibers and the shrinkage of the nanofibers, which affected the thickness during the crosslinking reaction[51] and helped the nanofibers retain their original shape.[52] Thus, we were able to enhance the utilization of the water-soluble polymer through crosslinking.

Swelling Ratio and Weight Loss

The PVA&SDP mat contained more water than the PVA&SDP@HNT mat. In the case of PVA&SDP@HNTs, the swelling ratio and weight loss decreased because of the presence of an HNT-filled space instead of water molecules. On the contrary, in PVA&SDP, the sole presence of SDP in the polymer matrix slightly increased the hydrophilicity of the mat; this involved the opening of the pore structures followed by an increase in the water penetration.[53] With this pattern, higher swelling ratios tended to be correlated with an increase in the weight loss. We concluded that when large amounts of water molecules were removed from the swelled electrospun nanofibers, they transformed the complex structure or reduced the inherent mass under dry conditions (Figure 7).

In Vitro Release of SDP

In vitro release was conducted to verify the loading and release performance of SDP from the HNTs as biocontainers. SDP was chosen as the model drug for the release profile in this study, either in pure form or embedded within HNTs to form SDP@HNT composites in PVA membrane. The release properties are an important parameter, which helped to elucidate the performance of the SDP compound and SDP@HNTs clusters by vacuum processing in the electrospun PVA matrix. Factors such as the crosslinking bonding, presence of HNTs, and preparation method of loading the drug into the HNTs heavily influenced the drug-release process. In this study, the effects of the HNT-loaded SDP and the crosslinking reaction were examined. Among the three types of nanofibers, the PVA nanofibrous mat was excluded.

In the noncrosslinked electrospun samples, the PVA&SDP and PVA&SDP@HNTs, the amounts of SDP released from each sample during the total given time interval (192 h) were about 80 and 60%, respectively. In the PVA&SDP nanofiber, SDP released rapidly within the first 12 h, and this depleted about 65% of the total drug content. The absence of HNTs indicated a faster drug release. On the contrary, for the PVA&SDP@HNTs, the total released amount of SDP was about 55%. As the time increased, the difference between the two samples' behaviors was seen to steadily increase. This was attributed to the presence of HNTs in the polymer complex structure. On the basis of this result, the HNTs induced a sustained drug release in the electrospun sample. Our drug-delivery system was similar to the core–shell delivery system because of the hollow cylindrical structure of the HNTs. PVA&SDP@HNT nanofibers acted as the core–shell threads and provided the sustained release.[54] The 20% difference in the total drug-release amount between the PVA&SDP and PVA&SDP@HNTs compensated for the effects of HNTs in the PVA&SDP@HNT complex nanofiber. Of the noncrosslinked samples, the difference in dissolution was the presence of HNTs. SDP was both loaded into HNTs and embedded with the surface of HNTs. When it was immersed in the medium, the freely SDP was released from the nanofibers but SDP incorporated with HNTs was slowly released. In the incorporated SDP with HNTs, SDP embedded with the surface of HNTs was first released; then, SDP was loaded into the lumen of the HNTs and subsequently released or encapsulated within the inner spaces.[55] In the case of the C PVA&SDP and C PVA&SDP@HNTs, a similar pattern appeared.

Crosslinking also induced sustained drug release. The reaction with GA reduced PVA's hydrophilicity through the replacement of its surface hydroxyl groups, which were hydrophilic by nature, with unreacted ends, intramolecular in the PVA chain and intermolecular among the PVA chains.[10] The modified

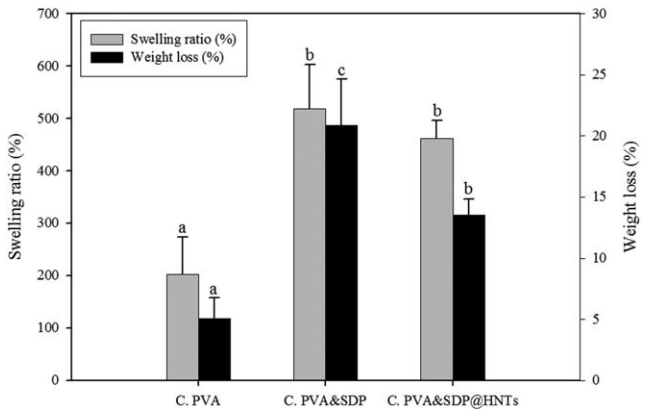

Figure 7. Swelling ratio and weight loss of the crosslinked nanofibrous mats. Different letters (a–c) within a column indicate significant differences ($p < 0.05$).

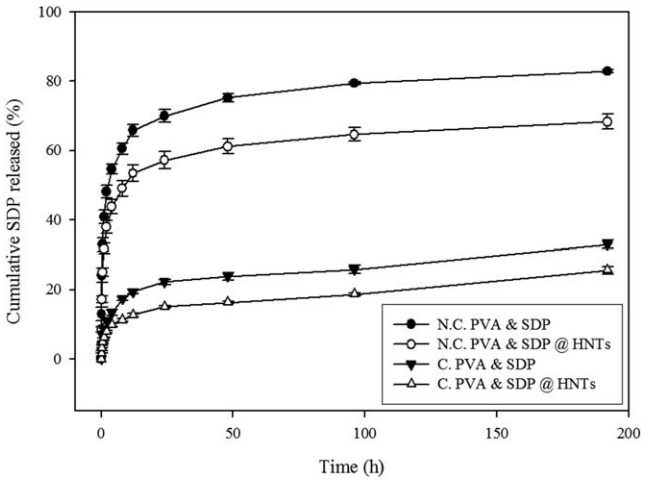

Figure 8. Cumulative SDP release profiles of the different nanofibers. Each data point indicates the mean plus or minus the standard deviation of the test results in triplicate. The electrospun samples were placed in PBS at 37°C.

nanofibrous mats slowed in drug release from the medium. This result is shown clearly in Figure 8.

After being closely checked in the medium, the C PVA&SDP and C PVA&SDP@HNTs retained their original formation. However, a portion of the PVA&SDP and PVA&SDP@HNTs collapsed and swelled, becoming opaque. The appearance of the nanofibrous mats demonstrated differences in the amount of drug released. Because drug release depends on the diffusion of the model drug and its disintegration from the outer shape of the polymer, we were able to conclude that less dramatic changes in the appearance of the original formation corresponded to lower levels of released drug.

A low initial burst and prolonged release of SDP resulted from this stepwise diffusion of the drug through two layers (HNTs and PVA) from the electrospun PVA&SDP@HNTs.[12] The noncrosslinked fibers' greater hydrophilicity induced a greater burst drug release than crosslinked fibers. Crosslinking slowed drug release by rendering the hydrophilicity of the pristine fiber mat into hydrophobicity. Thus, the hydroxyl groups in the C PVA&SDP@HNTs were less distributed than those in the C PVA&SDP, and the C PVA&SDP@HNTs were less affected by crosslinking. Therefore, we concluded that the difference in cumulative drug release between the C PVA&SDP and PVA&SDP@HNTs was smaller than that between the noncrosslinked poly(vinyl alcohol) and sodium D-pantothenate (NC PVA&SDP) and noncrosslinked sodium D-pantothenate loaded halloysite nanotubes (NC PVA&SDP@HNTs).

In conclusion, the presence of HNTs resulted in increases in the apparent density of the nanofibers and the density of the polymer solution. The increase in the viscosity of the PVA&SDP@HNTs resulted from packed SDP@HNTs in the polymer solution. In addition, the appearance of the polymer solution containing HNTs was opaque; this was in line with the good dispersion of HNTs in the polymer solution. The electrospun nanofibers filled with well-dispersed SDP@HNTs resulted in stronger interparticle interactions and followed the sustained release of SDP from HNTs. Similar effects of HNTs were reported by Qi *et al.*,[13] with a small diameter of HNTs in their delivery system.

In Vitro Release Kinetics of SDP

As shown in Table II, the Peppas parameter showed a value of less than 0.5; this was correlated with a Fickian diffusion mechanism. The crosslinked samples were too long to be released from the mats because of their semicrystalline state and change in structure, which occurred with the introduction of more hydrophobic moieties from the crosslinking agent.[56] The correlation coefficient of all of the samples ranged from 0.878 to 0.942; lower values were not satisfactory, but C PVA&SDP (coefficient of determination (r^2) = 0.9417) and C PVA&SDP@HNTs (r^2 = 0.9420) showed good correlation coefficients. In the polymeric matrix loading of the SDP and HNTs, we hypothesized a uniform distribution both outside and inside the fibers. This pattern included, first, the simple packaging of SDP and, second, the formation of SDP@HNT inclusions in the fibers. The degradation of the more hydrophilic noncrosslinked PVA&SDP and PVA&SDP@HNTs occurred gradually from the outermost surface of the matrix; this was followed by the release of the drug inside the PBS medium. Because of its hydrophilicity, SDP in noncrosslinked nanofibers was released more quickly than in those that had been crosslinked. This trend, observed in all of the samples, was traced by the sequential drug diffusion and degradation of the outermost surface of the polymer.[2]

CONCLUSIONS

By simple blend-electrospinning, we successfully fabricated PVA&SDP and PVA&SDP@HNT nanofibers with crosslinking. A mass ratio of 1.5:1 (SDP/HNTs) was determined to be optimal for the loading of SDP into the lumen of HNTs. The FTIR spectroscopy and XRD results verified the SDP and HNT good compatibility with PVA. There was little difference in the porosities among the noncrosslinked nanofibers. However, in the crosslinked nanofibers, the modified structure of the composite greatly influenced the porosity. The swelling properties and weight loss were quantitatively correlated with the *in vitro* drug-release rates. The drug-loading kinetics demonstrated that SDP release from all of the nanofibers depended on the diffusion caused by the deformation of polymer-based structures with relatively acceptable r^2 values (0.88–0.94) in the medium, where the original shapes of the crosslinked nanofibers were

Table II. Kinetic Parameters of SDP Release from Four Electrospun Nanofibers with the Peppas Equation

Formulations	Peppas parameter		Mechanism of release
	n	R^2	
NC PVA&SDP	0.235	0.8914	Fickian diffusion
NC PVA&SDP@HNTs	0.260	0.8778	Fickian diffusion
C PVA&SDP	0.312	0.9417	Fickian diffusion
C PVA&SDP@HNTs	0.306	0.9420	Fickian diffusion

maintained better than those of the noncrosslinked ones. The presence of HNTs as inclusions in the nanofibers and the crosslinking treatment induced and controlled the sustained drug release. Thus, the prepared PVA&SDP@HNT composite nanofibers, on the basis of environmentally friendly solvents, had a high potential for local drug delivery for the treatment of simple scars by the supplication and maintenance of moisture on human skin.

ACKNOWLEDGMENTS

This research was supported by the International Research and Development Program of the National Research Foundation of Korea, which is funded by the Ministry of Education, Science, and Technology of Korea (contract grant number 2012K1A3A1A20031356), by Korea University (through a grant), and by the Institute of Biomedical Science and Food Safety at the Korea University Food Safety Hall. The authors are very grateful to the Korea Basic Science Institute (Republic of Korea) for access to the X-ray diffractometer and for technical support.

REFERENCES

1. Shaikh, R. P.; Kumar, P.; Choonara, Y. E.; Du Toit, L. C.; Pillay, V. *Biofabrication* **2012**, *4*, 025002.
2. Hu, X.; Liu, S.; Zhou, G.; Huang, Y.; Xie, Z.; Jing, X. *J. Controlled Release* **2014**, *185*, 12.
3. Sharma, A.; Gupta, A.; Rath, G.; Goyal, A.; Mathurand, R.; Dhakate, S. *J. Mater. Chem. B* **2013**, *1*, 3410.
4. Bhardwaj, N.; Kundu, S. C. *Biotechnol. Adv.* **2010**, *28*, 325.
5. Jiang, J.; Xie, J.; Ma, B.; Bartlett, D.; Xu, A.; Wang, C.-H. *Acta Biomater.* **2014**, *10*, 1324.
6. Babar, A.; Pillai, J.; Plakogiannis, F. *Drug Dev. Ind. Pharm.* **1992**, *18*, 1823.
7. Robinson, J.; Lee, V. H. Controlled Drug Delivery: Fundamentals and Applications; Informa Health Care; New York, **1987**.
8. Canbolat, M. F.; Gera, N.; Tang, C.; Monian, B.; Rao, B. M.; Pourdeyhimi, B.; Khan, S. A. *ACS Appl. Mater. Interfaces* **2013**, *5*, 9349.
9. Wu, L.; Yuan, X.; Sheng, J. *J. Membr. Sci.* **2005**, *250*, 167.
10. Destaye, A. G.; Lin, C.-K.; Lee, C.-K. *ACS Appl. Mater. Interfaces* **2013**, *5*, 4745.
11. Kayaci, F.; Sen, H. S.; Durgun, E.; Uyar, T. *Food Res. Int.* **2014**, *62*, 424.
12. Hu, C.; Liu, S.; Zhang, Y.; Li, B.; Yang, H.; Fan, C.; Cui, W. *Acta Biomater.* **2013**, *9*, 7381.
13. Qi, R.; Guo, R.; Shen, M.; Cao, X.; Zhang, L.; Xu, J.; Yu, J.; Shi, X. *J. Mater. Chem.* **2010**, *20*, 10622.
14. Joussein, E.; Petit, S.; Churchman, J.; Theng, B.; Righi, D.; Delvaux, B. *Clay Miner.* **2005**, *40*, 383.
15. Lvov, Y. M.; Shchukin, D. G.; Mohwald, H.; Price, R. R. *ACS Nano* **2008**, *2*, 814.
16. Ghebaur, A.; Garea, S. A.; Iovu, H. *Int. J. Pharm.* **2012**, *436*, 568.
17. Zhai, R.; Zhang, B.; Liu, L.; Xie, Y.; Zhang, H.; Liu, J. *Catal. Commun.* **2010**, *12*, 259.
18. Abdullayev, E.; Lvov, Y. *J. Nanosci. Nanotechnol.* **2011**, *11*, 10007.
19. Shchukin, D. G.; Lamaka, S.; Yasakau, K.; Zheludkevich, M.; Ferreira, M.; Möhwald, H. *J. Phys. Chem. C* **2008**, *112*, 958.
20. Dhanaraju, M.; Sivakumar, V.; Subhashree, R.; Bhaskar, K. *Indian Drugs* **2002**, *39*, 222.
21. Schmidt, C.; Moll, F. *Pharm. Ind.* **1996**, *58*, 436.
22. Kumar, T. P.; Umesh, H.; Shivakumar, H.; Ravi, V.; Siddaramaiah. *J. Macromol. Sci. Pure Appl. Chem.* **2007**, *44*, 583.
23. Ding, B.; Kim, H. Y.; Lee, S. C.; Shao, C. L.; Lee, D. R.; Park, S. J.; Kwag, G. B.; Choi, K. J. *J. Polym. Sci. Part B: Polym. Phys.* **2002**, *40*, 1261.
24. Hassan, C. M.; Peppas, N. A. Biopolymers · PVA Hydrogels, Anionic Polymerisation, Nanocomposites; Springer: Berlin Heidelberg, **2000**; p 37.
25. Vidyalakshmi, K.; Rashmi, K.; Pramod Kumar, T.; Siddaramaiah. *J. Macromol. Sci. Chem.* **2004**, *41*, 1115.
26. Taepaiboon, P.; Rungsardthong, U.; Supaphol, P. *Nanotechnology* **2006**, *17*, 2317.
27. Aqil, M.; Sultana, Y.; Ali, A.; Dubey, K.; Najmi, A.; Pillai, K. *Drug Delivery* **2004**, *11*, 27.
28. Chun, M.-K.; Hossain, K.; Choi, S.-H.; Ban, S.-J.; Moon, H.; Choi, H.-K. *J. Pharm. Invest.* **2012**, *42*, 139.
29. Li, X.; Kanjwal, M. A.; Lin, L.; Chronakis, I. S. *Colloids Surf. B* **2013**, *103*, 182.
30. Biro, K.; Thaçi, D.; Ochsendorf, F. R.; Kaufmann, R.; Boehncke, W. H. *Contact Dermatitis* **2003**, *49*, 80.
31. Göbbels, M.; Gross, D. *Klin. Monatsblatter Augenheilkunde* **1995**, *209*, 84.
32. Ebner, F.; Heller, A.; Rippke, F.; Tausch, I. *Am. J. Clin. Dermatol.* **2002**, *3*, 427.
33. He, W.; Ma, Z.; Yong, T.; Teo, W. E.; Ramakrishna, S. *Biomaterials* **2005**, *26*, 7606.
34. Ma, Z.; Kotaki, M.; Yong, T.; He, W.; Ramakrishna, S. *Biomaterials* **2005**, *26*, 2527.
35. Jeong, S. I.; Krebs, M. D.; Bonino, C. A.; Samorezov, J. E.; Khan, S. A.; Alsberg, E. *Tissue Eng. Part A* **2010**, *17*, 59.
36. Costa, P.; Lobo, J. M. S. *Eur. J. Pharm. Sci.* **2001**, *13*, 123.
37. Oh, H. J.; Pant, H. R.; Kang, Y. S.; Jeon, K. S.; Pant, B.; Kim, C. S.; Kim, H. Y. *Polym. Int.* **2012**, *61*, 1675.
38. Fu, S.; Ni, P.; Wang, B.; Chu, B.; Peng, J.; Zheng, L.; Zhao, X.; Luo, F.; Wei, Y.; Qian, Z. *Biomaterials* **2012**, *33*, 8363.
39. Zhang, C.; Yuan, X.; Wu, L.; Han, Y.; Sheng, J. *Eur. Polym. J.* **2005**, *41*, 423.
40. Silverstein, R.; Webster, F. Spectrometric Identification of Organic Compounds; Wiley: Hoboken, NJ, **2006**.
41. Zhou, W. Y.; Guo, B.; Liu, M.; Liao, R.; Rabie, A. B. M.; Jia, D. *J. Biomed. Mater. Res. Part A* **2010**, *93*, 1574.
42. Shamsi, M. H.; Luqman, M.; Basarir, F.; Kim, J. S.; Yoon, T. H.; Geckeler, K. E. *Polym. Int.* **2010**, *59*, 1492.

43. Wang, Y.; Guo, G.; Chen, H.; Gao, X.; Fan, R.; Zhang, D.; Zhou, L. *Int. J. Nanomed.* **2014**, *9*, 1991.
44. Lambert, J. B.; Shurvell, H. F.; Lightner, D. A.; Cooks, R. G. Introduction to Organic Spectroscopy; Macmillan: New York, **1987**.
45. Podsiadlo, P.; Kaushik, A. K.; Arruda, E. M.; Waas, A. M.; Shim, B. S.; Xu, J.; Nandivada, H.; Pumplin, B. G.; Lahannand, J.; Ramamoorthy, A. *Science* **2007**, *318*, 80.
46. Churchman, G.; Theng, B. *Clay Miner.* **1984**, *19*, 161.
47. Guo, G.; Fu, S.; Zhou, L.; Liang, H.; Fan, M.; Luo, F.; Qian, Z.; Wei, Y. *Nanoscale* **2011**, *3*, 3825.
48. Touny, A. H.; Lawrence, J. G.; Jones, A. D.; Bhaduri, S. B. *J. Mater. Res.* **2010**, *25*, 857.
49. Hodge, R.; Edward, G. H.; Simon, G. P. *Polymer* **1996**, *37*, 1371.
50. Dong, Y.; Chaudhary, D.; Haroosh, H.; Bickford, T. *J. Mater. Sci.* **2011**, *46*, 6148.
51. Affandi, N. N.; Ahmad, M. R.; Baharudin, A.; Shukry, N. A. A. In 2012 IEEE Colloquium on Humanities, Science and Engineering (CHUSER); IEEE: Sabah, Malaysia, **2012**, p 458.
52. Liu, Y.; Bolger, B.; Cahill, P. A.; McGuinness, G. B. *Mater. Lett.* **2009**, *63*, 419.
53. Gilchrist, S. E.; Lange, D.; Letchford, K.; Bach, H.; Fazli, L.; Burt, H. M. *J. Controlled Release* **2013**, *170*, 64.
54. Ji, X.; Yang, W.; Wang, T.; Mao, C.; Guo, L.; Xiao, J.; He, N. *J. Biomed. Nanotechnol.* **2013**, *9*, 1672.
55. Kelly, H.; Deasy, P.; Ziaka, E.; Claffey, N. *Int. J. Pharm.* **2004**, *274*, 167.
56. Zamani, M.; Morshed, M.; Varshosaz, J.; Jannesari, M. *Eur. J. Pharm. Biopharm.* **2010**, *75*, 179.